Changes in the Zr environment in zirconia–silica xerogels with composition and heat treatment as revealed by Zr K-edge XANES and EXAFS

Gavin Mountjoy,*[a] David M. Pickup,[a] Ruth Anderson,[a] Graham W. Wallidge,[b] Mark A. Holland,[a] Robert J. Newport[a] and Mark E. Smith[b]

[a] School of Physical Sciences, University of Kent at Canterbury, Canterbury, UK CT2 7NR. E-mail: g.mountjoy@ukc.ac.uk; Fax: +44 (0)1227 827 558; Tel: +44 (0)1227 764 000 ext. 3776

[b] Department of Physics, University of Warwick, Coventry, UK CV4 7AL

X-ray absorption spectroscopy at the Zr K-edge is an important technique for probing the environment of Zr. Here it is applied to zirconia–silica xerogels with composition $0.07 \leqslant x \leqslant 0.40$, where x is the molar ratio Zr : (Zr + Si). Reference samples of crystalline ZrO_2, $ZrSiO_4$, $BaZrO_3$ and liquid Zr n-propoxide were also examined. New XANES (X-ray adsorption near edge structure) results are presented for zirconia–silica xerogels, and compared with previous EXAFS (extended X-ray absorption fine structure) results. For high Zr contents ($x = 0.4$) there is a separate, amorphous ZrO_2 phase, which before heat treatment is similar to Zr hydroxide, and after heat treatment at 750 °C is similar to an amorphous precursor of tetragonal ZrO_2. For low Zr contents ($x = 0.1$) there is atomic mixing of Zr in the SiO_2 network, and the environment of Zr is more similar to that in Zr n-propoxide compared to other reference samples. New in situ XANES and EXAFS results are presented for $x = 0.1$ xerogels heated at 250 °C. These clearly show that the Zr environment depends on ambient moisture in addition to heat treatment.

1. Introduction

Mixed zirconia–silica materials are technologically useful because of their strength, fracture toughness and chemical durability (like zirconia), low thermal expansion and tunable refractive index.[1] There is also interest in the possible catalytic applications of these materials.[2] The structure of mixed zirconia–silica materials is fundamentally interesting because Zr^{4+} cannot isomorphically substitute for Si^{4+} in silicate minerals, due to its large size (Zr–O coordination of 6–8) and high charge (compared to Mg^{2+} for example).[3] There is one mixed zirconia–silica crystalline compound, zircon ($ZrSiO_4$), but its formation requires heating at 1400 °C.[4] The preparation of mixed zirconia–silica glasses by melt-quenching is difficult because of the high melting temperatures required.[5]

Preparation by the sol–gel process has the advantage of using liquid precursors and is a comparatively low temperature process for producing glassy materials.[6] A gel is produced by hydrolysis and condensation reactions of metal alkoxide precursors, and is then converted to a xerogel by drying. A xerogel is generally an amorphous, microporous, hydrated solid, and becomes more like a conventional melt-quenched glass with heat treatment up to ~1000 °C. The structure of zirconia–silica xerogels is strongly dependent on the composition, preparation method and heat treatment. In order to understand better their properties, it is important to characterise the environment of Zr and how it depends on sample preparation conditions.

The atomic structure of amorphous zirconia–silica xerogels with composition $0 < x \leqslant 0.5$, where x is the molar ratio Zr : (Zr + Si), has been investigated using several techniques. IR,[7,8] Raman[7] and ^{29}Si NMR[8] studies show that Zr disrupts the SiO_2 network. ^{17}O NMR studies for $x = 0.1$[8] show a predominance of Si–O–Zr oxygen configurations, whilst for $x = 0.4$[8] they show significant amounts of O exclusively bonded to Zr, i.e. O–Zr_n configurations, which before heat

treatment are similar to those in monoclinic ZrO_2 (m-ZrO_2[9]). For $x < 0.1$, IR and Raman studies[7] have concluded that the Zr local environment is like that in cubic ZrO_2 (c-ZrO_2[9]). X-ray diffraction studies have shown that continued heat treatment of zirconia–silica xerogels with $x \leqslant 0.5$ eventually causes crystallisation of tetragonal ZrO_2[10] (t-ZrO_2[9]). X-ray and neutron diffraction[11] and Zr K-edge EXAFS (extended X-ray absorption fine structure)[8,11] results are consistent with all of these observations. Previous workers[12] have suggested that for $0.3 < x < 0.5$ the local structure is similar to $ZrSiO_4$, but $ZrSiO_4$ contains only isolated SiO_4 tetrahedra,[4] which is completely inconsistent with ^{29}Si NMR observations of zirconia–silica xerogels.[8]

We have previously presented a combined IR, ^{29}Si and ^{17}O NMR and Zr K-edge EXAFS study carried out on a single set of zirconia–silica xerogel samples.[8] Here we present new EXAFS and XANES (X-ray absorption near edge structure) results, including in situ measurements, which greatly extend the previous work. This leads to a more detailed description of the Zr environment in $x = 0.1$ xerogels, and clearly shows that it is sensitive to ambient moisture.

2. Method

2.1. Sample preparation

Our xerogel samples were prepared using the sol–gel process from the following precursors: tetraethyl orthosilicate, TEOS (Aldrich, 98%), and Zr(IV) n-propoxide, $Zr(OPr^n)_4$ (70 wt.% solution in propan-1-ol, Aldrich). HCl (Fisons) was used as a catalyst and propan-1-ol (Aldrich, 99+%) was used as a mutual solvent.

The method of Yoldas[13] was used to promote homogeneity within the samples. This involved prehydrolysis of the TEOS to maximise the number of Si–OH groups, before mixing with the more reactive $Zr(OPr^n)_4$ precursor. The chosen pre-

DOI: 10.1039/a910300g

Phys. Chem. Chem. Phys., 2000, 2, 2455–2460   2455

hydrolysis conditions were TEOS : propan-1-ol : water in a 1 : 1 : 1 molar ratio in the presence of HCl (pH 1), stirring for 2 h. The appropriate quantity of stock $Zr(OPr^n)_4$–propan-1-ol solution was diluted further, 1 : 4 by volume with propan-1-ol, before being slowly added to the prehydrolysed TEOS solution with stirring. After one hour, water was added such that the overall alkoxide : water molar ratio was 2. The resulting clear sol was then left to gel: this typically took a few days, depending on composition. This method of preparation is hereafter referred to as method A.

A second set of samples was made in the same way, but with stock $Zr(OPr^n)_4$–propan-1-ol solution diluted further, 1 : 30 by volume with propan-1-ol, in an effort to promote greater mixing. This is hereafter referred to as method B.

All samples were air dried for several days, finely ground, and then pumped under vacuum for 24 h to remove any excess solvent. Heat treatments were performed at a heating rate of 5 °C min^{-1} with each temperature maintained for 2 h.

Various reference compounds were also examined. Samples of m-ZrO_2, t-ZrO_2 and c-ZrO_2, were obtained from the TOSOH Corporation. The t-ZrO_2 and c-ZrO_2 were stabilised with 3 and 13 mol% Y_2O_3,[14] hereafter denoted " st-ZrO_2 " and " sc-ZrO_2 " respectively. Samples of $BaZrO_3$ and Zr n-propoxide were obtained from Aldrich, and a sample of $ZrSiO_4$ was obtained from Strem Chemicals. A sample of Zr hydroxide was prepared by the precipitation method. $ZrCl_2 \cdot 8H_2O$ (50 g) was dissolved in distilled water (200 ml) to produce zirconium hydroxide precipitate and ammonium chloride. The precipitation reaction was halted by adding 35 wt.% aqueous ammonia until a pH of ~ 10 was reached, with the aim of producing small precipitate particles. The precipitate was washed with water and filtrated, then heated to 230 °C to remove excess water.

2.2. Experiment

We have previously presented EXAFS results for zirconia–silica xerogels prepared using method A, and for reference compounds of st-ZrO_2, m-ZrO_2 and $ZrSiO_4$.[8] Here we present new EXAFS results for reference compounds of sc-ZrO_2, $BaZrO_3$ and Zr n-propoxide, and for an unheated $x = 0.1$ xerogel measured *in situ* at 25 and at 250 °C. The experiments were carried out on EXAFS station 9.2 at the Daresbury Laboratory, UK. EXAFS spectra were collected in transmission mode at the Zr K-edge, with edge position $E_0 = 17998$ eV. A Si(220) monochromator was used, with a harmonic rejection of 50%, and a resolution of ~ 5 eV at the Zr K-edge.[15]

The absorbance, $\mu t = \ln(I_t/I_0)$, was measured using standard ion chambers before and after the sample (I_0 and I_t respectively). *In situ* measurements were carried out using a furnace with kapton windows and an N_2 atmosphere.[16] The pre- and post-edge backgrounds, μt_{pre} and μt_{post}, were obtained by fitting polynomials of order 1 and 3 respectively. The normalised absorbance is $1 + \chi = (\mu t - \mu t_{pre})/(\mu t_{post} - \mu t_{pre})$.

In our previous study, XANES results were not presented. Here we present XANES results for all of the samples studied by EXAFS, plus additional samples. Most of the XANES experiments were carried out on EXAFS station 9.2 as described above. XANES spectra were collected in the near edge region, from -15 to $+30$ eV with steps of 0.6 eV relative to the absorption edge. The limited lifetime of the core-hole causes a broadening of ~ 2 eV at the Zr K-edge.[17] XANES spectra are presented with $E = 0$ at the inflection point of the main absorption edge ($E_0 = 17998$ eV). For the Zr hydroxide sample, the combined XRD/EXAFS station 9.3 was used. The experimental conditions were similar to those described above except that XANES spectra were collected with steps of 1.7 eV.

2.3. EXAFS data analysis

The EXAFS spectra were analysed using the curved wave, single-scattering, equation[18]

$$\chi(k) = S_0(k)^2 \sum_j \frac{N_j}{kR_j^2} |f(k, R_j)| e^{-2R_j/\lambda(k)}$$
$$\times e^{-2\sigma_j^2 k^2} \sin(2kR_j + 2\delta(k) + \phi(k, R_j)) \qquad (1)$$

where k is the photoelectron wavevector, and N_j, R_j and σ_j describe the coordination number, distance and standard deviation (respectively) for the jth shell of neighbouring atoms around the central atom. The program EXCURV92[19] was used to fit eqn. (1) to the experimental $\chi(k)$. The parameters $|f(k, R_j)|$, $\phi(k, R_j)$, $\delta(k)$ and $\lambda(k)$ represent the amplitude and phase of backscattering, the phase shift at the central atom, and the inelastic mean free path of the photoelectron. These parameters were calculated within EXCURV92 using von Barth and Hedin–Lundqvist potentials, with $Z + 1$ approximation for the excited atom. The amplitude reduction factor, $S_0(k)^2$, represents multi-electron effects. EXCURV92 uses an additional parameter, E_F, to correct the edge position E_0. Eqn. (1) does not include the effects of multiple-scattering. However, multiple scattering is expected to be less significant for amorphous materials (as seen in amorphous Si[20]), and should not affect results for nearest neighbour, *i.e.* Zr–O, correlations.

Structural parameters were obtained from the experimental $\chi(k)$ using least squares fitting in k-space with k^3 weighting. The fits for crystalline compounds were carried out with N_j fixed equal to the published values, and R_j, σ_j, E_F and $S_0(k)^2$ free to vary. The value of $S_0(k)^2$ was found to be 1.0. The fits for the xerogel samples were carried out with fixed $S_0(k)^2 = 1.0$, and N_j, R_j, σ_j and E_F free to vary. The data from the xerogel samples, which have weaker EXAFS oscillations, are significantly affected by a double-electron transition at ~ 7.7 Å^{-1}.[21] Consequently, during the fitting for these samples, the data between 7.0 and 8.3 Å^{-1} were excluded. The statistical errors of fitting are obtained from the 95% confidence limits in the least sum of squares.[22] The quality of fits is reported using the discrepancy index

$$R_{dis} = \left(\sum_i k_i^3 |\chi(k_i)_{expt} - \chi(k_i)_{fit}| \right) \bigg/ \sum_j k_i^3 |\chi(k_i)_{expt}| \times 100\% \qquad (2)$$

Values of $k_{min} = 2.8$ Å^{-1} and $k_{max} \approx 20$ Å^{-1} were used for all samples, except the $x = 0.1$ xerogel measured *in situ*, for which $k_{max} \approx 16$ Å^{-1}.

2.4. XANES data analysis

XANES at the K-edge involves the excitation of a 1s photoelectron into low-lying empty states at the central atom with p-type symmetry.[23] The characteristic features of XANES spectra for transition metal oxides are as follows.[24] Pre-edge peak(s) correspond to 1s to nd transitions with p–d mixing. Such transitions are not allowed for completely centrosymmetric metal atom sites, but the pre-edge peak intensity increases as the degree of centrosymmetry decreases. The shape of the main absorption peak represents transitions to np continuum states and " shape resonances " of the metal atom environment.[23] Peaks occurring a few 10 eV about the main peak correspond to multiple scattering involving second nearest neighbour atoms or higher shells. Qualitative information can be obtained by comparing XANES spectra with those of reference compounds (the so-called " fingerprint " method) [*e.g.* ref. 25].
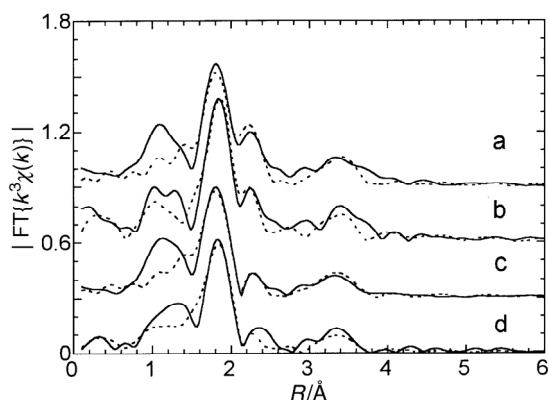
3. Results

3.1. EXAFS results

To assist in the interpretation of results, Table 1 describes the environments of Zr in various reference compounds. Pure t-ZrO_2 and c-ZrO_2 are unstable at 25 °C,[9] and Table 1 shows instead st-ZrO_2 and sc-ZrO_2, i.e. the forms stabilised with Y_2O_3.[14] The EXAFS results for reference compounds are also shown in Table 1. There is good agreement with the crystallographic data and with other EXAFS studies, with the following exceptions. For m-ZrO_2 the observed value of R_{Zr-O} is slightly shorter than the crystallographic value, an effect which has previously been explained.[26] For st-ZrO_2 and sc-ZrO_2, the observed values of R_{Zr-Oa} and R_{Zr-Ob} differ from values reported elsewhere, probably due to differences in details of stabilisation by Y_2O_3. Attempts to fit the $ZrSiO_4$ EXAFS data with a second Zr–Si correlation at ~3.6 Å did not yield the correct Zr–Si distance. This occurs because Si is a weak backscatterer, and hence such correlations do not make a strong contribution to the EXAFS signal. The values of R_{dis} for $BaZrO_3$ are high because there are strong correlations at larger distances (these were not fitted because it is the Zr–O correlations which are of interest here).

Figs. 1 and 2 show experimental $k^3\chi(k)$ and the magnitude of the FT of $k^3\chi(k)$ previously measured *ex situ* for $x = 0.1$ xerogels before and after heat treatment at 750 °C. Figs. 1 and 2 also show new *in situ* measurements for an unheated $x = 0.1$ xerogel measured *in situ* at 25 and at 250 °C. The FTs show features at ~1.5 Å which are unphysical, being too short for a realistic values of R_{Zr-O}. Similar artefacts have been observed in Zr and Ti K-edge EXAFS.[21,27] Table 2 shows the EXAFS results for the xerogel sample measured *in situ*, along with previous results for zirconia–silica xerogels with $x = 0.1$ and $x = 0.4$ measured *ex situ*. It was previously shown that for $x = 0.1$ it is necessary to use a split Zr–O shell to obtain a satisfactory fit, but for $x \geqslant 0.2$, a single Zr–O shell is sufficient.
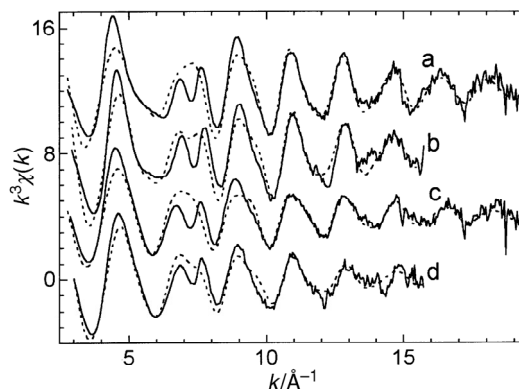
Fig. 1 $k^3\chi(k)$ for $x = 0.1$ xerogels measured *ex situ* (a) before and (c) after heat treatment at 750 °C,[8] and measured *in situ* (b) at 25 °C and (d) at 250 °C. Dotted lines are fits to the data.

Fig. 2 $|FT\{k^3\chi(k)\}|$ corresponding to Fig. 1. Dotted lines are fits to the data. (Note that for (a) and (c) fitting was performed using $k_{max} \sim 20$ Å^{-1} but the FT is displayed using $k_{max} \sim 16$ Å^{-1}, so that FT effects are the same as for (b) and (d).)

Table 1 EXAFS results[a] for reference compounds from the literature[b] and in our work[c] (where EXAFS results were not available, X-ray diffraction results are shown[d])

Compound [ref.]	Correlation	Literature N	Literature R/Å	Our work R/Å	$2\sigma^2$/Å^2	R_{dis} (%)
st-ZrO_2^* [9]	Zr–Oa	4	2.08	2.09(1)	0.010(2)	39
	Zr–Ob	4	2.38	2.28(3)	0.046(15)	
			{2.23}			
	Zr–Zr	12	3.62	3.62(1)	0.018(1)	
$ZrSiO_4$ [4]	Zr–Oa	4	2.13	2.12(1)	0.005(2)	38
	Zr–Ob	4	2.27	2.26(1)	0.006(2)	
			{2.20}			
	Zr–Si	2	2.99	3.00(1)	0.005(2)	
	Zr–Zr	4	3.63	3.64(1)	0.006(1)	
sc-ZrO_2^* [9]	Zr–Oa	3	2.04	2.11(1)	0.008(1)	26
	Zr–Ob	4	2.28	2.21(1)	0.020(5)	
			{2.15}			
	Zr–Zr	12	3.64	3.60(1)	0.021(2)	
m-ZrO_2 [9]	Zr–O	7	2.16	2.13(1)	0.019(2)	36
	Zr–Zr	7	3.45	3.46(1)	0.013(1)	
	Zr–Zr	4	3.98	3.99(1)	0.018(3)	
Zr hydroxide [32]	Zr–O	7	2.14	—	—	
Zirconolite [26]	Zr–O	7	2.16	—	—	
$BaZrO_3$ [40]	Zr–O	6	2.09	2.06(1)	0.007(4)	47
	Zr–Ba	8	3.62	3.59(1)	0.014(5)	
	Zr–Zr	6	4.18	4.23(2)	0.003(1)	
Zr n-propoxide [37]	Zr–Oa	2	1.96	1.97(1)	0.008(2)	35
	Zr–Ob	4	2.18	2.19(3)	0.017(4)	
			{2.11}			
	Zr–Zr	1	3.53	3.52(1)	0.014(9)	
	Zr–C	6	3.54	3.62(3)	0.016(15)	

[a] { } Denotes average of R_{Zr-Oa} and R_{Zr-Ob}. * Denotes samples stablised with Y_2O_3. [b] Refs. 9, 26, 32 and 37. [c] Ref. 8 and this study. [d] Refs. 4 and 40.

Table 2 EXAFS results[a] for zirconia–silica xerogels prepared using method A[b]

x	Heat treatment/°C	Correlation	N	R/Å	$2\sigma^2/\text{Å}^2$	R_{dis}
0.4	None	Zr–O	7.9(5)	2.14(1)	0.023(2)	30
		Zr–Zr	4.2(15)	3.49(1)	0.025(5)	
0.4	750	Zr–O	7.4(5)	2.12(1)	0.028(2)	32
		Zr–Zr	4.3(16)	3.40(1)	0.030(5)	
0.1	None	Zr–Oa	3.1(4)	2.00(1)	0.006(1)	35
		Zr–Ob	6.4(13)	2.25(1)	0.031(1)	
				{2.17(1)}		
		Zr–Zr	0.7(4)	3.37(1)	0.012(6)	
0.1	750	Zr–Oa	2.4(8)	1.98(1)	0.007(2)	31
		Zr–Ob	4.4(4)	2.15(4)	0.039(17)	
				{2.09(4)}		
		Zr–Zr	0.5(4)	3.38(2)	0.013(7)	
0.1	25*	Zr–Oa	3.3(5)	2.00(1)	0.008(3)	37
		Zr–Ob	5.1(13)	2.23(1)	0.023(7)	
				{2.14(1)}		
		Zr–Zr	1.2(8)	3.35(2)	0.016(9)	
0.1	250*	Zr–Oa	2.5(8)	1.99(1)	0.010(3)	38
		Zr–Ob	4.6(10)	2.18(2)	0.039(15)	
				{2.11(2)}		
		Zr–Zr	0.9(7)	3.34(2)	0.019(9)	

[a] { } Denotes average of $R_{Zr–Oa}$ and $R_{Zr–Ob}$. * Denotes previously unheated sample measured *in situ*. [b] Ref. 8 and this study.

No reliable Zr–Si correlation was obtained from the EXAFS fitting. This is particularly surprising because such correlations are expected for low Zr content. Indeed, ^{17}O NMR studies[8] have shown that Zr–O–Si configurations are prevalent for x = 0.1 xerogels. One factor is that Si is a weak backscatterer. Another is that the xerogels are amorphous, and structural disorder will cause large values of $2\sigma^2_{Zr–Si}$. In fact, fitting with fixed $N_{Zr–Si} = 4$ typically gives values of $R_{Zr–Si} = 3.80 \pm 0.05$ Å and $2\sigma^2_{Zr–Si} = 0.06 \pm 0.05$ Å^2. In our previous EXAFS study,[8] it was also not possible to extract meaningful Zr–Si correlations. In contrast, for ZrSiO$_4$ there is very little structural disorder, *i.e.* $2\sigma^2_{Zr–Si} = 0.006$ Å^2, and Zr–Si correlations are obtained from the EXAFS fitting.

3.2. XANES results

Fig. 3a shows the XANES spectra for reference compounds. These are in good agreement with those reported in the literature.[9,14,28,29] Also included is a result from the literature for annealed zirconolite (CaZrTi$_2$O$_7$).[26] There are pre-edge features (see left arrow) due to 1s–4d transitions. This corresponds to p–d mixing, and such mixing has been shown in density of states calculations for crystalline ZrO$_2$[30] (7- and 8-fold coordination) and Y$_2$O$_3$[31] (6-fold coordination). The pre-edge feature is strongest for st-ZrO$_2$ which has a Zr site with strong tetrahedral distortion, *i.e.* reduced centrosymmetry.[14] Different shapes are seen for the main absorption edge (see Fig. 3a): a double peak for sites with tetrahedral distortion ((1) ZrSiO$_4$, (2) st-ZrO$_2$ and (3) sc-ZrO$_2$), a single peak for sites with 7-fold coordination without Zr–O splitting ((4) m-ZrO$_2$, (5) Zr hydroxide and (6) zirconolite), and a double peak for sites with octahedral coordination ((7) BaZrO$_3$ and (8) Zr n-propoxide). A secondary peak at ⩾40 eV above the edge (see right arrow) corresponds to multiple scattering due to strong Zr–Zr or Zr–Ba correlations (see Table 1). The XANES for Zr hydroxide are similar to that for m-ZrO$_2$, which is consistent with a report that in Zr hydroxide the Zr local environment is similar to that in m-ZrO$_2$.[32]

Fig. 3b shows the XANES spectra of unheated zirconia–silica xerogels prepared using method A. With increasing Zr content, the main absorption edge clearly changes from being asymmetric with peak on the right-hand side, to being asymmetric with peak on the left-hand side. This clear trend in the XANES spectra implies the presence of at least two different Zr environments. This obviously parallels the change in EXAFS results from a split Zr–O correlation for x ⩽ 0.1 to a

single Zr–O correlation for x ⩾ 0.2 (see Table 2). Fig. 4a shows that the change occurs more slowly for samples prepared using method B compared to method A (see Fig. 3b). As these samples have the same Zr contents, the difference must be due to method B giving a more homogeneous distribution of Zr. This may be expected, because in method B there is greater pre-hydrolysis of silica and greater dilution of Zr with propanol.

Fig. 4b shows the effect of heat treatment on XANES spectra for xerogel samples prepared using method A. There is substantial change in the XANES spectra from before (dotted lines) to after (solid lines) heat treatment at 750 °C. In particular, xerogels with x = 0.1 heat treated at 750 °C show a pronounced growth of the pre-edge feature due to 1s–4d transitions (see arrow in Fig. 4b). Fig. 5 shows the XANES spectra for x = 0.1 xerogels prepared using method A before and after heat treatment at 250 °C measured *in situ* at 25 and 250 °C. For measurements *in situ* at 250 °C there is pronounced growth of the pre-edge feature.
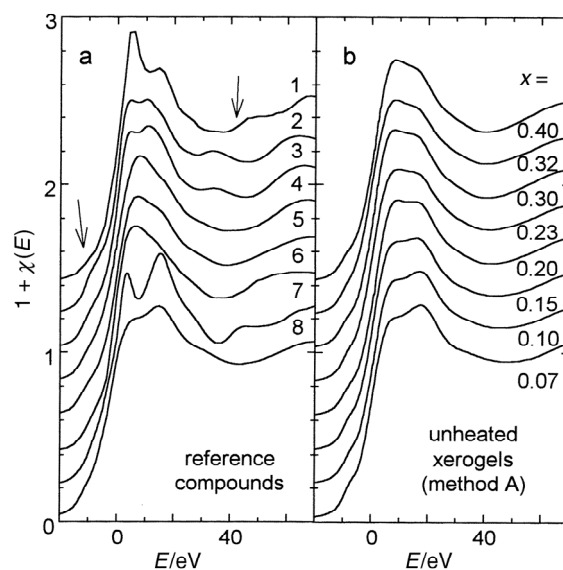
Fig. 3 (a) XANES spectra of reference compounds: (1) ZrSiO$_4$, (2) st-ZrO$_2$, (3) sc-ZrO$_2$, (4) Zr hydroxide, (5) m-ZrO$_2$, (6) zirconolite,[26] (7) BaZrO$_3$ and (8) Zr n-propoxide. (Left and right arrows indicate features corresponding to 1s–4d transitions and multiple scattering respectively.) (b) XANES spectra of unheated zirconia–silica xerogels prepared using method A.
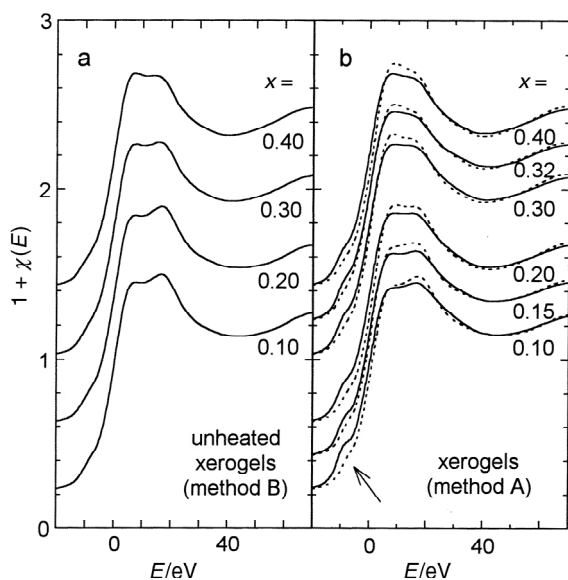
Fig. 4 (a) XANES spectra of unheated xerogels prepared using method B. (b) XANES spectra of xerogels prepared using method A before (dotted lines) and after (solid lines) heat treatment at 750 °C.

4. Discussion

4.1. Zirconia–silica xerogels with high Zr content

The XANES spectrum for the unheated $x = 0.4$ xerogel is most similar to that for Zr hydroxide. The most reasonable interpretation is that for unheated xerogels with $x = 0.4$, most of the Zr is present in a separate, amorphous ZrO_2 phase which is very similar to Zr hydroxide. This is consistent with the EXAFS results which show significant Zr–O–Zr correlations, no significant splitting of Zr–O correlations, and N_{Zr-O} and R_{Zr-O} corresponding to a 7-fold coordination, indicating a Zr local environment similar to that in m-ZrO_2.[8,32] The similar EXAFS results for samples with $0.2 \leqslant x \leqslant 0.3$ indicate a predominance of phase separated ZrO_2 in these samples, but the XANES spectra show that there is an increasing contribution from a second, different Zr environment as x decreases (see below).

The XANES spectra for $x = 0.4$ shows pronounced changes after heat treatment at 750 °C, which are very similar to the changes observed for Zr hydroxide during heat treatment
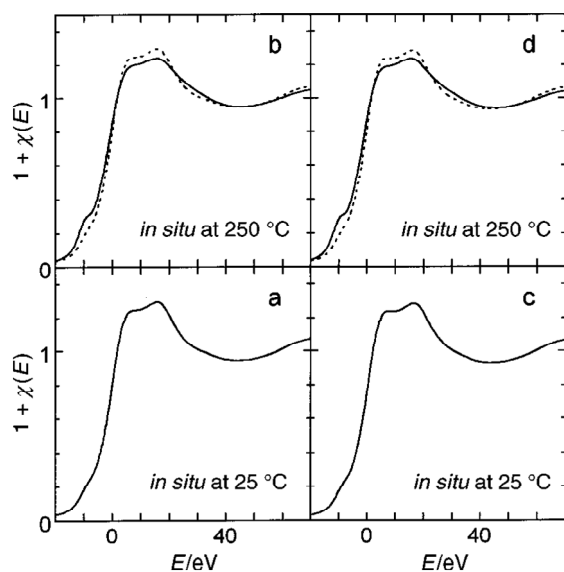

Fig. 5 XANES spectra of $x = 0.1$ xerogels (a, b and dotted lines) before and (c, d) after heat treatment at 250 °C, measured (a, c) *in situ* at 25 °C and (b, d) *in situ* at 250 °C.

prior to the crystallisation of st-ZrO_2.[33] This indicates the development of an amorphous precursor to st-ZrO_2, and is consistent with ^{17}O NMR results which show O–Zr_n configurations becoming more like those in st-ZrO_2 after heat treatment at 750 °C.[8] ^{17}O NMR results[8] indicate roughly similar proportions of Si–O–Zr and O–Zr_n configurations for $x = 0.4$ after heat treatment at 750 °C. Assuming these correspond to the boundaries and interiors (respectively) of the ZrO_2 phase, the typical size of such regions can be estimated to be a few nm in diameter. Note that additional heat treatment eventually causes the crystallisation of t-ZrO_2, a phase which is known to be stabilised by small domain size.[34]

4.2. Zirconia–silica xerogels with low Zr content

The EXAFS results for the unheated $x = 0.1$ xerogel indicate the presence of less than one Zr–O–Zr correlation per Zr, which is consistent with ^{17}O NMR studies that show Si–O–Zr configurations are much more prevalent than O–Zr_n configurations.[8] Hence, while there may be some Zr–Zr clustering, there is not a separate ZrO_2 phase. The absence of phase separation is consistent with other observations of the zirconia–silica system. When molten $ZrSiO_4$ is rapidly quenched, separate zirconia-rich and silica-rich phases are formed, with the latter containing <15 mol% ZrO_2.[5] X-ray diffraction studies of zirconia–silica xerogels show that crystallisation is substantially retarded for $x \leqslant 0.15$.[10] In $x = 0.1$ xerogels the Zr environment is obviously dominated by Zr–O–Si correlations. However, the details of Si–O–Zr configurations are not obvious because they involve both Si–O bond valences which are ≈ 1.0 and Zr–O bond valences which are <1 (necessary in order for Zr to have coordination of $\geqslant 6$).[35]

The EXAFS results for the unheated $x = 0.1$ xerogel (see Table 2) show a pronounced splitting of the Zr–O correlation, with mean $R_{Zr-O} = 2.17$ Å, which suggests a Zr local environment with 7-fold coordination similar to that in sc-ZrO_2. However, this interpretation is difficult to apply in detail, given that sc-ZrO_2 contains only O–Zr_n configurations and these are largely absent from the xerogel. Raman studies have also concluded the Zr local environment in heat treated xerogels with $x < 0.1$ is like that in sc-ZrO_2,[7] but those studies noted that similar Raman features occur in perovskites, in which Zr has octahedral coordination.

The XANES spectrum for the unheated $x = 0.1$ xerogel has a main absorption peak which is very similar to that for Zr n-propoxide. Zr n-propoxide contains Zr–O–R, R–OZr_2 and Zr–(ROH) configurations (see Fig. 6a).[36] These provide a basis for describing oxygen configurations in the xerogel, with R replaced by H or Si. The EXAFS results give values of R_{Zr-Oa} and R_{Zr-Ob} slightly longer than those for Zr n-propoxide,[37] total $N_{Zr-O} > 6$, and mean $R_{Zr-O} = 2.14 \pm 0.01$ Å which is longer than for 6-fold coordination. Hence the EXAFS and XANES together imply a Zr environment similar to that in Zr n-propoxide, but with greater than 6-fold coordination. This could occur if there is an additional, weakly bound ligand, such as a water group. Such additional ligands have been proposed for Zr in Zr hydroxide[32] (see Fig. 6b). The reason is that Zr in an octahedral environment is coordinatively unsaturated. In addition, the EXAFS results for
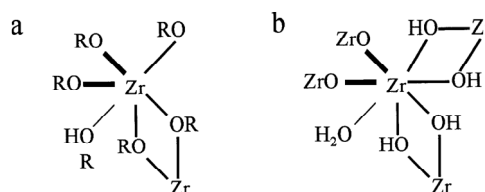

Fig. 6 Local environments of Zr observed in (a) Zr n-propoxide,[36,37] and proposed for (b) Zr hydroxide.[32] (Line thickness represents bond valences of approximately 1.0, 0.5 and <0.5, in descending order.)

$x = 0.1$ xerogels indicate approximately one Zr–O–Zr correlation per Zr which is similar to the dimers present in Zr n-propoxide.

4.3. Effects of heating

Heat treatment of the $x = 0.1$ xerogel at $750\,^{\circ}C$ causes small but significant changes in the EXAFS results (see Table 2). The Zr–O correlation continues to be split, but R_{Zr-Ob} has decreased to 2.15 ± 0.04 Å, which is closer to that in Zr n-propoxide.[37] In addition, total N_{Zr-O} decreases and mean R_{Zr-O} decreases to 2.11 ± 0.02 Å which is shorter than for 7-fold coordination. Heat treatment at $750\,^{\circ}C$ results in XANES spectra with a pronounced pre-edge feature corresponding to 1s–4d transitions (see arrow in Fig. 4b), which is stronger than for any other samples. It is known in the case of Ti[38] an increase in 1s–3d transitions can result from distorted octahedral coordination. Hence the EXAFS and XANES results indicate that heat treatment at $750\,^{\circ}C$ generates a Zr environment similar to that in Zr n-propoxide but with increased octahedral distortion (see Fig. 6b). Heat treatment is expected to cause the loss of loosely bound ligands such as water groups.

We now turn our attention to the results of *in situ* measurements. As anticipated, the EXAFS and XANES results for an unheated $x = 0.1$ xerogel measured *ex situ*, and measured *in situ* at $25\,^{\circ}C$ are in good agreement (see Figs. 1, 2, 3b, and 5a). This shows reproducibility and that the effect of the furnace container is negligible. The EXAFS and XANES results for an unheated $x = 0.1$ xerogel measured *in situ* after 20 min at $250\,^{\circ}C$ are very similar to those measured *ex situ* after heat treatment at $750\,^{\circ}C$ for 2 h (see Figs. 1, 2, 4b, and 5b). In particular, the XANES show a pronounced pre-edge feature due to 1s–4d transitions. Furthermore, the same XANES features are also observed *in situ* at $250\,^{\circ}C$ for an $x = 0.1$ xerogel which has previously been heat treated at $250\,^{\circ}C$ for 2 h (see Figs. 5c and 5d). Hence the change in coordination must be due to the effects of ambient moisture. This is consistent with the presence of Zr–Ob correlations due to the water groups which are lost with heat treatment. The changes are irreversible at $750\,^{\circ}C$, presumably due to relaxation of the xerogel network structure associated with decreased porosity.

5. Conclusions

The Zr K-edge XANES study presented here provides a valuable addition to previous studies of zirconia–silica xerogels. For $x = 0.4$ there is a separate, amorphous ZrO_2 phase. The XANES results show that the ZrO_2 phase is initially similar to Zr hydroxide, and with heat treatment up to $750\,^{\circ}C$ becomes similar to an amorphous precursor of t-ZrO_2. For $x = 0.1$ there is atomic mixing of Zr in the SiO_2 network, and the Zr local environment has previously been described as similar to that in c-ZrO_2. However, the XANES and EXAFS results here show that it is more appropriately described as being similar to that in Zr n-propoxide, with significant changes occurring during heat treatment up to $750\,^{\circ}C$. The *in situ* XANES and EXAFS results for $x = 0.1$ xerogels clearly show rapid and reversible changes in the Zr environment with heating at $250\,^{\circ}C$, indicating Zr coordination is sensitive to ambient moisture. The change is irreversible with heat treatment at $750\,^{\circ}C$. This parallels results previously obtained for titania–silica xerogels.[39] In both cases the transition metal is coordinatively unsaturated due to the constraints of the SiO_2 network, and ambient moisture provides a way of increasing coordination.

References

1 M. Nogami, *J. Non-Cryst. Solids*, 1985, **69**, 415.
2 J. B. Miller and E. I. Ko, *J. Catal.*, 1996, **159**, 58.
3 R. Gill, in *Chemical fundamentals of Geology*, Unwin Hyman, London, 1989, ch. 9.
4 R. M. Hazen and L. W. Finger, *Am. Mineral.*, 1979, **64**, 157.
5 A. M. Evans, J. P. H. Williamson and F. P. Glasser, *J. Mater. Sci.*, 1980, **15**, 2325.
6 C. J. Brinker and G. W. Scherer, in *Sol-gel science: the physics and chemistry of sol-gel processing*, Academic Press, San Diego, 1990.
7 S. W. Lee and R. A. Condrate, *J. Mater. Sci.*, 1988, **23**, 2951.
8 D. M. Pickup, G. Mountjoy, G. W. Wallidge, R. J. Newport and M. E. Smith, *Phys. Chem. Chem. Phys.*, 1999, **1**, 2527.
9 P. Li, I.-W. Chen and J. E. Penner-Hahn, *Phys. Rev. B*, 1993, **48**, 10063.
10 K. Kamiya, S. Sakka and Y. Tatemichi, *J. Mater. Sci.*, 1980, **15**, 1765.
11 R. Anderson, G. Mountjoy, R. J. Newport and M. E. Smith, *J. Phys.: Condens. Matter*, 2000, in the press.
12 O. Stachs, T. Gerber and V. Petkov, *J. Mater. Sci.*, 1997, **32**, 4209.
13 B. E. Yoldas, *J. Non-Cryst. Solids*, 1980, **38–39**, 81.
14 P. Li, I.-W. Chen and J. E. Penner-Hahn, *Phys. Rev. B*, 1993, **48**, 10074.
15 F. J. W. Mosselmans, Daresbury Laboratory, 1999, unpublished result.
16 A. J. Dent, G. N. Greaves, M. A. Roberts, G. Sankar, P. A. Wright, R. H. Jones, M. Sheeny, D. Madill, C. R. A. Catlow, J. M. Thomas and T. Rayment, *Nucl. Instrum. Methods Phys. Res., B*, 1995, **97**, 20.
17 B. K. Teo, in *EXAFS: basic principles and data analysis*, Springer-Verlag, Berlin, 1986, p. 76.
18 J. Mustre de Leon, S. I. Zabinsky and R. C. Albers, *Phys. Rev. B*, 1995, **52**, 2995.
19 N. Binsted, J. W. Campbell, S. J. Gurman and P. C. Stephenson, *CCLRC Daresbury Laboratory EXCURV92 program*, 1991.
20 A. Bianconi, A. Di Cicco, N. V. Pavel, M. Benfatto, A. Marcelli, C. R. Natoli, P. Pianetta and J. Woicik, *Phys. Rev. B*, 1987, **36**, 6426.
21 W.-C. Wang and Y. Chen, *Phys. Status Solidi A*, 1998, **168**, 351.
22 R. W. Joyner, K. J. Martin and P. Meehan, *J. Phys. C.: Solid State Phys.*, 1987, **20**, 4005.
23 A. Bianconi, in *X-ray absorption: principles, applications, techniques of EXAFS, SEXAFS and XANES*, ed. D. C. Koninbsberger and R. Prins, Wiley, New York, 1987, ch. 11.
24 L. A. Grunes, *Phys. Rev. B*, 1983, **27**, 2111.
25 R. Brydson, L. A. J. Garvie, A. J. Craven, H. Sauer, F. Hofer and G. Cressey, *J. Phys. Condens. Matter*, 1993, **5**, 9379.
26 F. Farges, R. C. Ewing and G. E. Brown, *J. Mater. Res.*, 1993, **8**, 1983.
27 G. Antonioli, P. P. Lottici, I. Manzini, G. Gnappi, A. Montenero, F. Paloschi and P. Parent, *J. Non-Cryst. Solids*, 1994, **77**, p. 179.
28 F. Farges, G. E. Brown and D. Velde, *Am. Mineral.*, 1994, **79**, 838.
29 C. Sanchez and M. In, *J. Non-Cryst. Solids*, 1992, **147–148**, 1.
30 F. Follet, C. Noguera, N. Thromat, M. Gautier and J. P. Durand, *Phys. Rev. B*, 1990, **42**, 7587.
31 R. H. French, S. J. Glass, F. S. Ohuchi, Y.-N. Xu and W. Y. Ching, *Phys. Rev. B*, 1994, **49**, 5133.
32 X. Turrillas, P. Barnes, A. J. Dent, S. L. Jones and C. J. Norman, *J. Mater. Chem.*, 1993, **3**, 583.
33 A. V. Chadwick, V. M. Nield, I. J. F. Poplett, M. G. Tucker, G. Mountjoy and M. E. Smith, 2000, in preparation.
34 R. C. Garvie, *J. Phys. Chem.*, 1978, **82**, 218.
35 F. Farges, C. W. Ponader and G. E. Brown, *Geochim. Cosmochim. Acta*, 1991, **55**, 1563.
36 B. A. Vaatstra, J. C. Huffman, P. S. Gradeff, G. Hubert-Pfalzgraf, J.-C. Daran, S. Parraud, K. Yunlu and K. G. Caulton, *Inorg. Chem.*, 1990, **29**, 3126.
37 U. Reinohl, T. S. Ertel, W. Horner, A. Weber and H. Bertagnolli, *Ber. Bunsen-Ges. Phys. Chem.*, 1998, **102**, 144.
38 G. A. Waychunas, *Am. Mineral.*, 1987, **72**, 89.
39 G. Mountjoy, D. M. Pickup, G. W. Wallidge, R. Anderson, J. M. Cole, R. J. Newport and M. E. Smith, *Chem. Mater.*, 1999, **11**, 1253.
40 H. D. Megaw, *Proc. Phys. Soc. London*, 1946, **58**, 133.